

Supporting Information

for

Microscopic insight into the shaping of MOFs and its impact on CO₂ capture performance

Supriyo Naskar¹, Dong Fan¹, Aziz Ghoufi², Guillaume Maurin^{1*}

1. ICGM, Université de Montpellier, CNRS, ENSCM, Montpellier, 34293, France

*2. Institut de Physique de Rennes, IPR, UMR CNRS 6251, 263 Avenue du Général Leclerc,
35042 Rennes, France.*

* Corresponding author, Email: guillaume.maurin1@umontpellier.fr

Model of carboxymethyl cellulose (CMC)

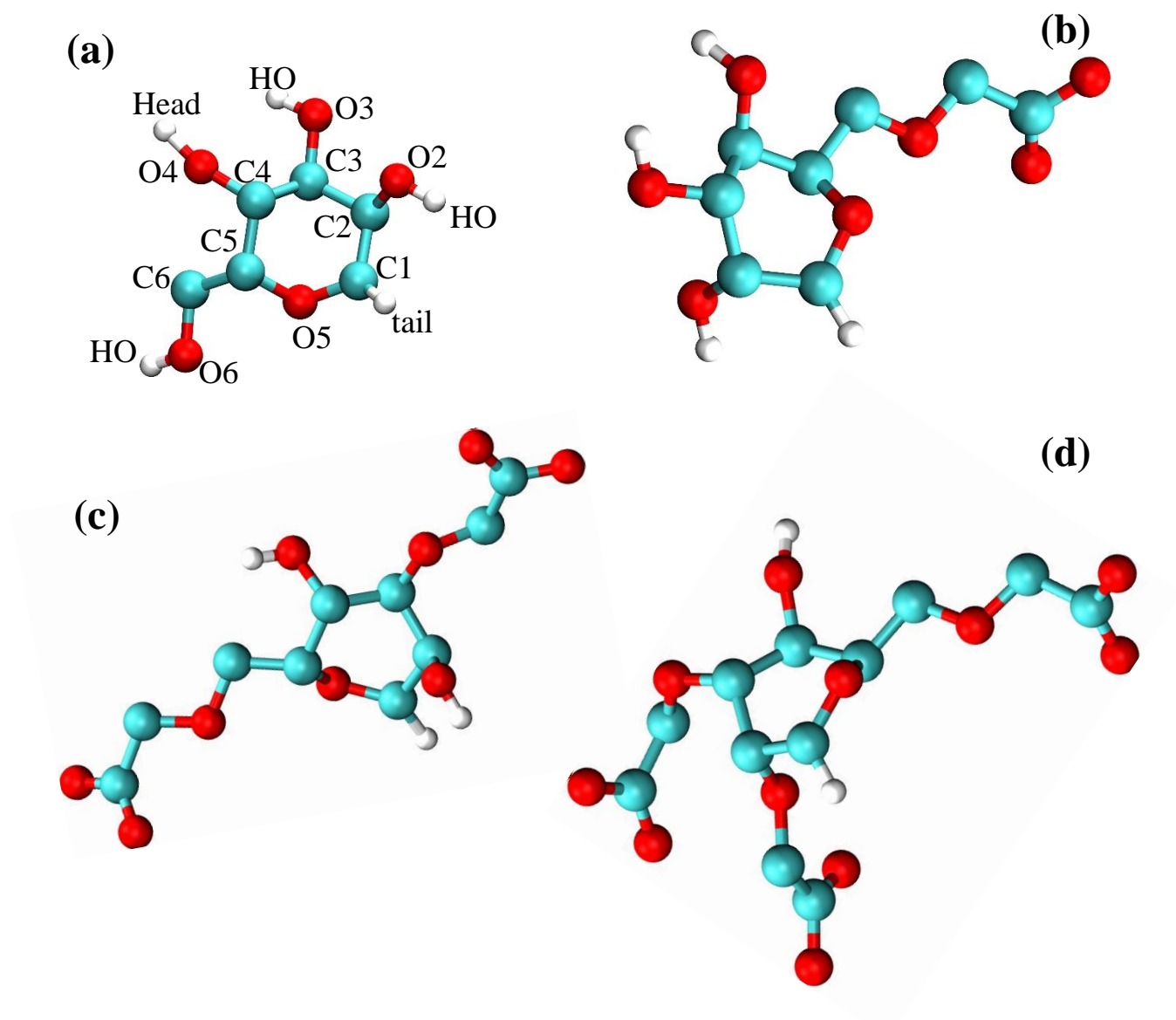


Figure S1 | Model of CMC monomer with different carboxymethyl group substitution. CMC monomer with (a) no carboxymethyl group, (b) one carboxymethyl group, (c) two carboxymethyl group, (d) three carboxymethyl group. Monomers are randomly chosen to build the final polymer. Panel a also represents the atom type to define the force-field in the next section. All the structures were geometry optimized at the DFT level as described in the main text.

Table S1 | Force-field parameters for carboxymethyl cellulose.

Non bonded Parameters for CMC *				
Name	Type	σ [Å]	ϵ (kcal/mol)	Charge [e]
C	COO ⁻	3.3611	0.097	0.2700
CH ₁	O-C1-O	3.8004	0.075	0.4000
	C2-OH, C3-OH	3.8004	0.075	0.1500
	C4-OR ₂ , C5-C-OH	3.8004	0.075	0.1600
CH ₂	R-CH ₂ -OH, R-CH ₂ -O-CH ₂ -COO ⁻ , R-CH ₂ -O-CH ₂ -COO ⁻	3.9199	0.117	0.1500
	R-O-CH ₂ -COO ⁻	3.9199	0.117	0.2080
O	-O-H	2.8706	0.241	-0.5480
	-O-H (chain end)	2.8706	0.241	-0.5730
	R-O-CH ₂ , R-CH ₂ -O-CH ₂ -COO ⁻	2.8706	0.241	-0.3580
	R-O-R (ether)	2.8706	0.241	-0.3600
	-COO ⁻	2.6259	0.412	-0.6350
HO	-O-H	0.0000	0.000	0.3980
H	-O-H (chain end)	0.0000	0.000	0.3730
Na ⁺	Ion to neutralize the charge of COO ⁻	2.7300	0.086	1.0000

* Bonded parameters are taken from work by Biermann et al.¹

Model of Poly (vinyl acetate) (PVA) monomer

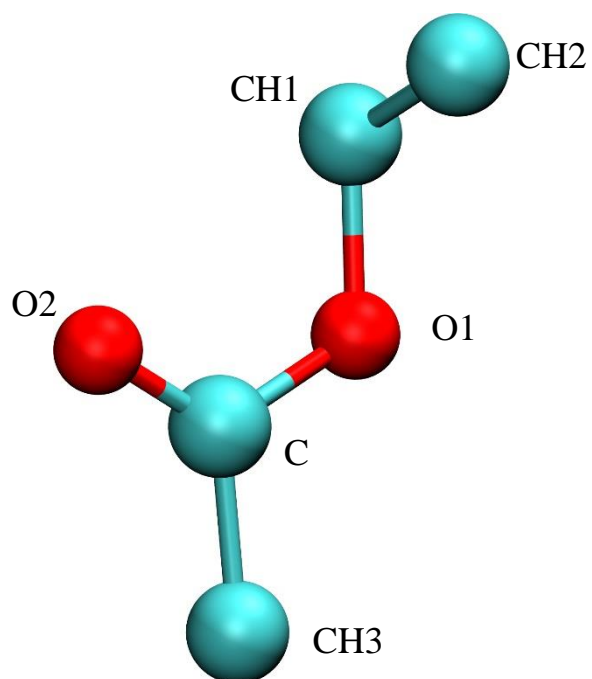


Figure S2 | Model of PVA monomer. The atom types are also described to define the force-field in the next section. This structure was geometry optimized at the DFT level.

Table S2 | Force-field parameters for PVA.

Non bonded Parameters for PVA *

Name	Type	σ [Å]	ϵ (kcal/mol)	Charge [e]
C	CH1	3.830	0.1184	0.261
C	CH2	3.675	0.1690	-0.076
O	O1	2.28	0.1093	-0.363
O	O2	3.05	0.1567	-0.505
C	C	3.90	0.0814	0.757
C	CH3	3.75	0.1947	-0.074

* Bonded parameters are taken from the work by Dong et al.²

Model of Poly (vinyl alcohol) (PVOH) monomer

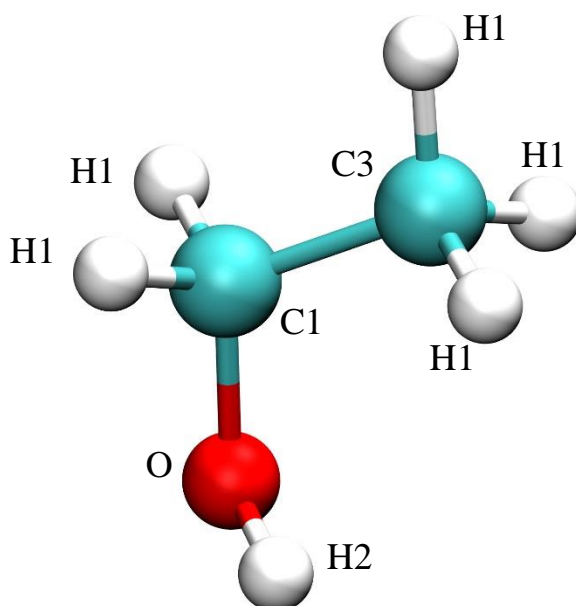


Figure S3 | Model of PVOH monomer. The atom types are also described to define the force-field in the next section. The structure is geometry optimized at the DFT-level.

Table S3 | Force-field parameters for poly (vinyl alcohol) (PVOH).

Non bonded Parameters for PVA*				
Name	Type	σ [Å]	ϵ (kcal/mol)	Charge [e]
C	C1	0.020	2.273	0.14
C	C3	0.080	2.060	-0.27
H	H1	0.022	1.319	0.09
H	H2	0.046	0.224	0.43
O	OH	0.152	1.768	-0.66
C	C2 (Chain end)	0.055	2.178	-0.18

* Bonded parameters are taken from the work by Semino et al.³

Model of Poly (vinyl butyral) (PVB) monomer

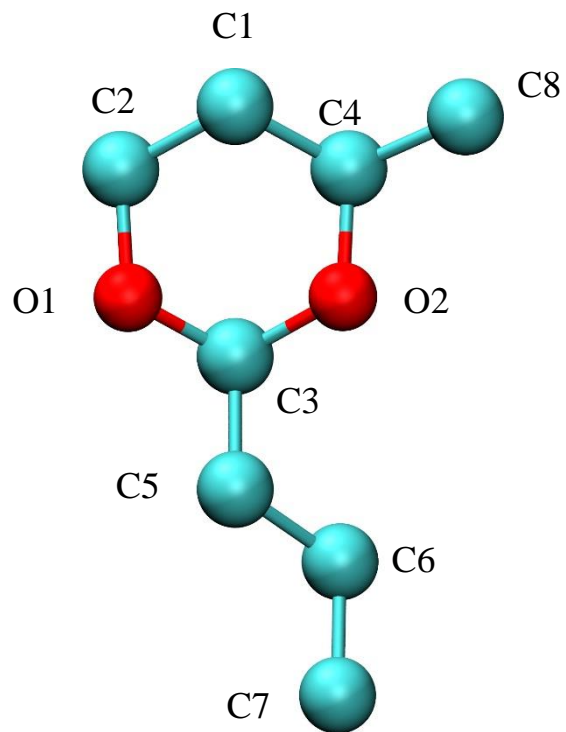


Figure S4 | Model of PVB monomer. The atom types are also described to define the force-field in the next section. The structure is geometry optimized at the DFT-level.

Table S4 | Force-field parameters for PVB.

Non bonded Parameters for PVB *				
Name	Type	σ [Å]	ϵ (kcal/mol)	Charge [e]
C	C1	3.91	0.104330	-0.112130
C	C2	3.91	0.104330	0.279604
C	C3	3.91	0.104330	0.420373
C	C4	3.91	0.104330	0.453536
C	C5	3.95	0.091411	-0.041533
C	C6	3.95	0.091411	0.141925
C	C7	3.75	0.194746	-0.073014
C	C8	3.95	0.091411	-0.084294
O	O1	2.39	0.308017	-0.479750
O	O2	2.39	0.308017	-0.504718

* Bonded parameters are taken from the GAFF AMBER force-field⁴.

Table S5 | System details of CMC, PVA, PVB, and PVOH binders with different chain length distribution

Name	System type	Chain length Distribution	Number of atoms
CMC	System 1	500	10054
	System 2	48,48,41,41,40,34,33,33,32,28,27,26,19,17,13,10,10	9854
	System 3	33,28,27,26,19,13,10	3130
PVA	System 1	500	3000
	System 2	49,48,36,36,35,34,32,30,28,28,27,22,20,17,16,15,14,13	3000
	System 3	49,44,42,36,32,31,31,30,29,28,26,21,20,20,18,15,14,13,12	3066
PVB	System 1	500	5000
	System 2	47,44,39,37,36,35,32,29,29,27,27,24,23,19,18,12,12,10	5000
	System 3	50,39,39,39,28,23,22,19,18,17,14	3080
PVOH	System 1	500	3508
	System 2	48,47,38,36,35,35,32,28,26,26,25,23,21,19,17,16,15,13	3644
	System 3	49,45,44,39,37,37,35,33,29,29,29,28,28,27,26,25, 24,23,22,22,21,21,20,19,19,18,17,17,16,16,16,15, 14,14,13,13,12,11,11,11,11,10,10	7176

Table S6 | Details of the thermodynamic parameters used during the 21 steps MD simulations for the equilibration of the binder density.

MD Step	Ensemble	T (K)	P (kbar)	Length (ps)
1	NVT	600		50
2	NVT	300		50
3	NPT	300	1	50
4	NVT	600		50
5	NVT	300		100
6	NPT	300	30	50
7	NVT	600		50
8	NVT	300		100
9	NPT	300	50	50
10	NVT	600		50
11	NVT	300		100
12	NPT	300	25	5
13	NVT	600		5
14	NVT	300		10
15	NPT	300	5	5
16	NVT	600		5
17	NVT	300		10
18	NPT	300	0.5	5
19	NVT	600		5
20	NVT	300		10
21	NPT	300	0.001	800

A note on the 21 steps MD simulations for the generation of equilibrated binder model.

The 21 molecular dynamics steps procedure is a well-established method for mimicking equilibrated and densely packed polymer melts to construct reliable atomistic models that accurately reproduce the experimental features of these polymers (density, pore distribution, Pair Distribution Function....). This computational strategy has been widely established and validated by the modelling community working in the polymer field. To summarize, initial work for the generation of polymer melts by Hofmann et al. referred to as the 12-step scheme, involved iterative application until reaching a consistent density⁵. Subsequently, Karayannis et al. expanded upon the 12-step scheme by incorporating annealing and decompression steps⁶. Later, Larsen et al. presented a novel generic scheme strategy inspired by Karayannis et al., termed the 21-step compression/relaxation scheme, which compresses and relaxes structures to experimental densities⁷. The final density was found to be independent of the temperature and pressure chosen for compression and decompression for all investigated polymers. Indeed, in our study, we choose the standard values of the temperature and pressure, described in the original paper ($T_{\max}=600\text{K}$ and $P_{\max}=50\text{Kbar}$). A clear benefit of the method is its speed when taking into account the relaxation times of dense glassy structures. We can summarize the major advantages of this method as follows: (a) the creation of an ensemble of equilibrated glassy polymer structures (final NPT MD simulation stage), with a density in line with the experimental value; (b) Initial simulation at high temperature and pressure generates configuration very fast as equilibration is much easier to achieve. The successive cooling steps generate uncorrelated melt configurations down to the glassy state which are representative of the synthesized polymers obtained in this experimental condition.”

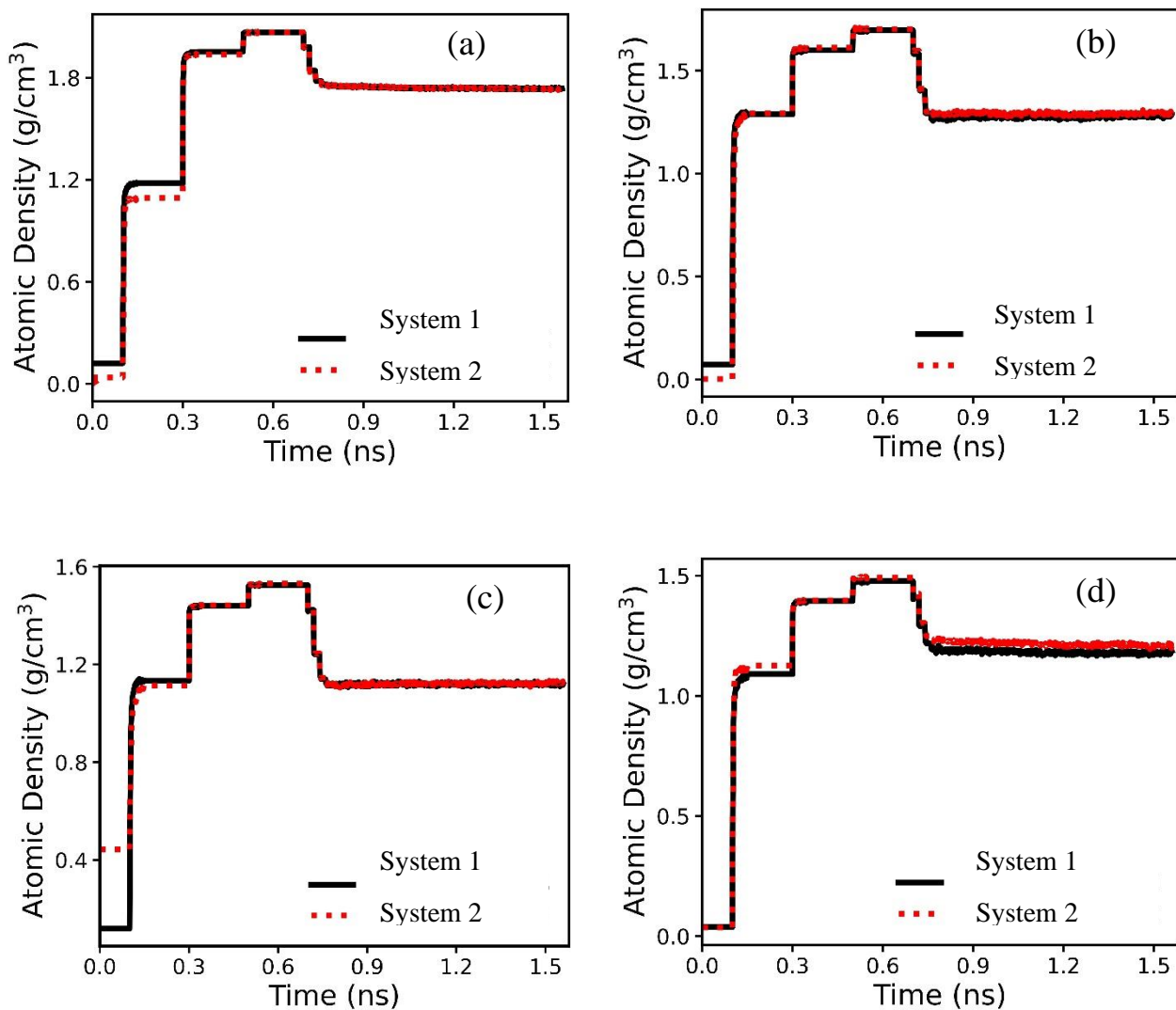


Figure S5 | Time evolution of the density for (a) CMC, (b) PVA, (c) PVB, and (d) PVOH binders with different chain length distributions (System 1 and System 2 as defined in Table S5) during the 21 steps MD equilibration. Results were independent of chain size and dispersity.

Table S7 | Density of CMC, PVA, PVB, and PVOH binders with different chain length distribution*

Name	System type	Simulated Density (g/cm ³)	Experimental Density (g/cm ³)
CMC	System 1	1.74 ± 0.004	
	System 2	1.74 ± 0.003	1.6-1.7 ^{8,9}
	System 3	1.72 ± 0.005	
PVA	System 1	1.28 ± 0.006	
	System 2	1.29 ± 0.005	1.19-1.26 ^{10,11}
	System 3	1.28 ± 0.006	
PVB	System 1	1.12 ± 0.004	
	System 2	1.12 ± 0.004	1.08-1.12 ¹²
	System 3	1.12 ± 0.004	
PVOH	System 1	1.18 ± 0.005	
	System 2	1.21 ± 0.006	1.19-1.3 ^{11,13}
	System 3	1.17 ± 0.005	

*Definition of the System 1, System 2, System 3 is given in the table S5. Results were independent of chain size and dispersity.

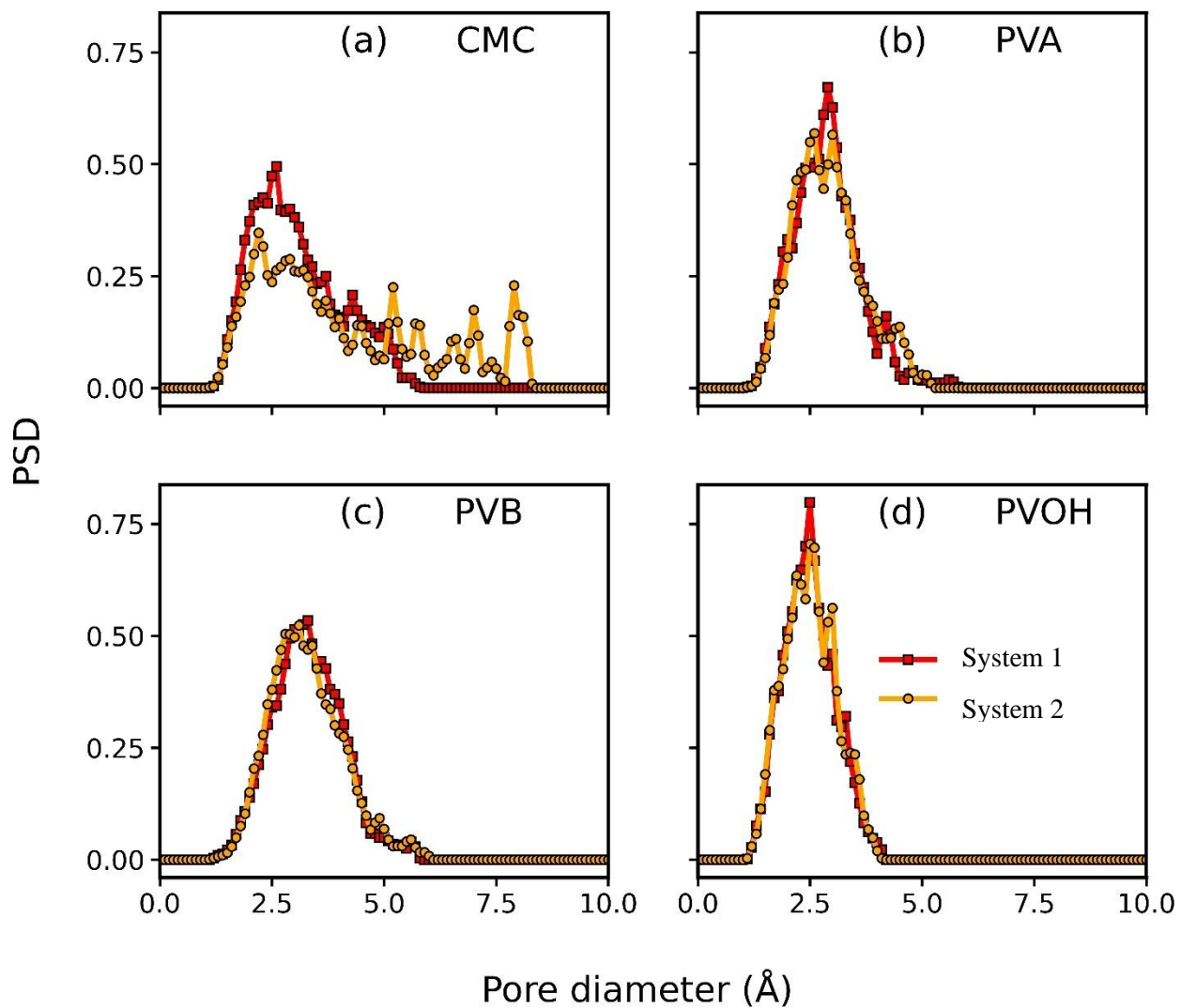


Figure S6 | Pore size distribution of (a) CMC, (b) PVA, (c) PVB, and (d) PVOH binders with different chain length distributions (System 1 and System 2 as defined in Table S5). Results were independent of chain size and dispersity.

Table S8 | Simulated mechanical properties of the binders. Mechanical properties were calculated using elastic deformation method as implemented in the LAMMPS software.

System	CMC	PVA	PVB	PVOH
Bulk Modulus (GPa)	12.86 ± 1.48	3.93 ± 1.15	3.39 ± 0.99	6.51 ± 0.75
Young Modulus (GPa)	11.15 ± 2.35	1.64 ± 0.78	1.66 ± 1.04	5.23 ± 0.76
Experimental values of Young Modulus (GPa)	8.7 ¹⁴ 11.34 ¹⁵	1.47 ¹⁶ 0.75 ¹⁷	0.95 ¹⁸ 1.31 ¹⁹	1.50-3.75 at 373 K ²⁰ 2.8-3.5 at 353 K ²¹

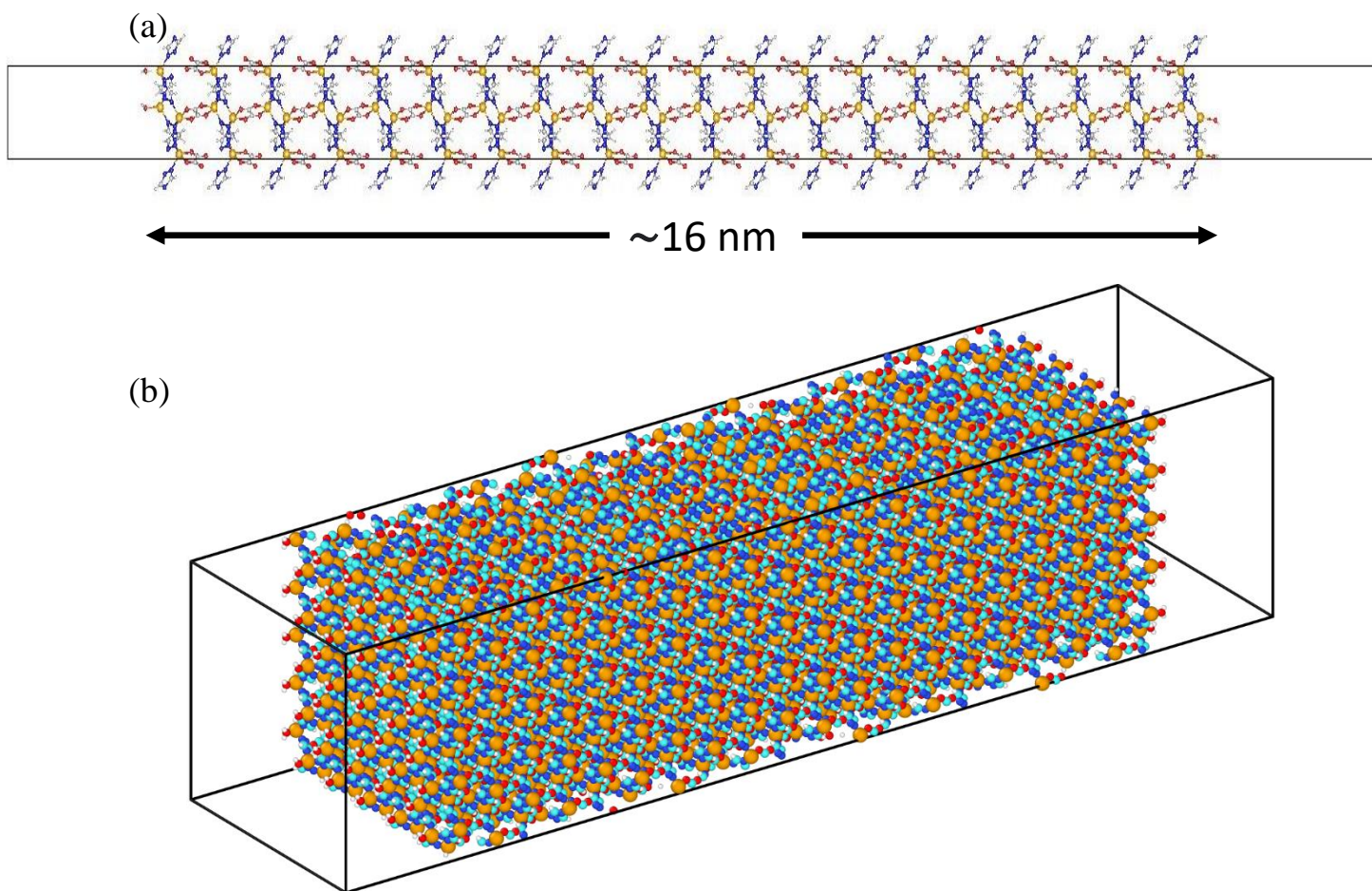


Figure S7 | Illustration of the slab surface (100) model of CALF-20. (a) Unit cell of the structure which is geometry optimized in CP2K software. (b) Supercell of the previous structure with $5 \times 5 \times 1$ repetition. Box dimension of the structure is $48.47 \times 47.42 \times 200 \text{ \AA}^3$. Color scheme: Zn, Orange; O, red; N, blue; C, cyan; H, white.

Table S9 | Lattice parameters of the DFT optimized and experimental CALF-20 bulk structure.

	a [Å]	b [Å]	c [Å]	α [°]	β [°]	γ [°]	V [Å ³]
DFT-D3	9.05545	9.89713	9.37722	90	117.6191	90	744.64739
Exp. ²²	8.91380	9.69350	9.48360	90	115.8950	90	737.16411

Table S10 | Universal force-field (UFF)²³ parameters for CALF-20 used in the GCMC and MD simulations.

Lennard-Jones Parameters		
Atom	ϵ (kcal/mol)	σ (Å)
Zn	0.124	2.4616
N	0.069	3.2607
O	0.06	3.1181
C	0.105	3.4309
H	0.044	2.5711

Modified Equilibrium Bond Distance *		
Bond type	r_0 [original]	r_0 [modified]
Zn – N	1.88	2.04
Zn – O	1.84	2.12
Zn - O_{water}	1.82	2.17

* Rest of the bonded parameters are same as UFF force-field.

Table S11 | Equilibrium bond distances of the CALF-20 structure using original and modified UFF force-field parameters in MD simulations and comparison with the DFT-optimized geometric features.

Equilibrium Bond Distance of the Bulk CALF-20				
Bond Type	DFT (VASP)		UFF (modified)	UFF (Original)
Zn-N	2.04 ± 0.04		2.04 ± 0.04	2.02 ± 0.04
Zn-O	2.12 ± 0.10		2.11 ± 0.04	1.98 ± 0.04
N-N	1.37 ± 0.00		1.34 ± 0.02	1.36 ± 0.02
N-C	1.34 ± 0.01		1.33 ± 0.02	1.35 ± 0.02
O-C	1.27 ± 0.01		1.30 ± 0.03	1.32 ± 0.02
C-H	1.08 ± 0.00		1.08 ± 0.03	1.08 ± 0.03
C-C	1.56 ± 0.00		1.45 ± 0.04	1.38 ± 0.04

Equilibrium Bond Distance of the geometry optimized CALF-20 (100) surface slab model				
Bond Type	DFT (VASP)	DFT (CP2K)	UFF (modified)	UFF (Original)
Zn-N	2.04 ± 0.04	2.04 ± 0.03	2.04 ± 0.04	1.94 ± 0.05
Zn-O	2.12 ± 0.10	2.12 ± 0.10	2.12 ± 0.04	1.90 ± 0.05
Zn-O_{water}	2.17 ± 0.06	2.16 ± 0.06	2.14 ± 0.04	1.80 ± 0.06
N-N	1.37 ± 0.00	1.36 ± 0.00	1.33 ± 0.02	1.33 ± 0.02
N-C	1.34 ± 0.01	1.33 ± 0.01	1.35 ± 0.02	1.35 ± 0.02
O-C	1.27 ± 0.01	1.26 ± 0.01	1.30 ± 0.03	1.29 ± 0.02
O_{water}-H_{water}	0.99 ± 0.00	0.99 ± 0.00	0.99 ± 0.02	0.99 ± 0.02
C-H	1.08 ± 0.00	1.08 ± 0.00	1.08 ± 0.03	1.08 ± 0.03
C-C	1.56 ± 0.00	1.55 ± 0.00	1.44 ± 0.04	1.37 ± 0.03

Table S12 | Calculated relative surface energies of different CALF-20 slab surfaces.

Surfaces	(1 0 0)	(1 1 0)	(1 0 1)
$\Delta \Phi_{sur}$ [J m ⁻²]	0.00	+0.84	+0.32

Table S13 | Details of the thermodynamic parameters used during the 21 steps MD simulations for the equilibration of the MOF/Binder Composite. P_z refers to pressure coupling along the z-direction only.

MD Step	Ensemble	T (K)	P_z (kbar)	Length (ps)
1	NVT	600		50
2	NVT	300		50
3	NP_zT	300	1	50
4	NVT	600		50
5	NVT	300		100
6	NP_zT	300	30	50
7	NVT	600		50
8	NVT	300		100
9	NP_zT	300	50	50
10	NVT	600		50
11	NVT	300		100
12	NP_zT	300	25	5
13	NVT	600		5
14	NVT	300		10
15	NP_zT	300	5	5
16	NVT	600		5
17	NVT	300		10
18	NP_zT	300	0.5	5
19	NVT	600		5
20	NVT	300		10
21	NP_zT	300	0.001	800

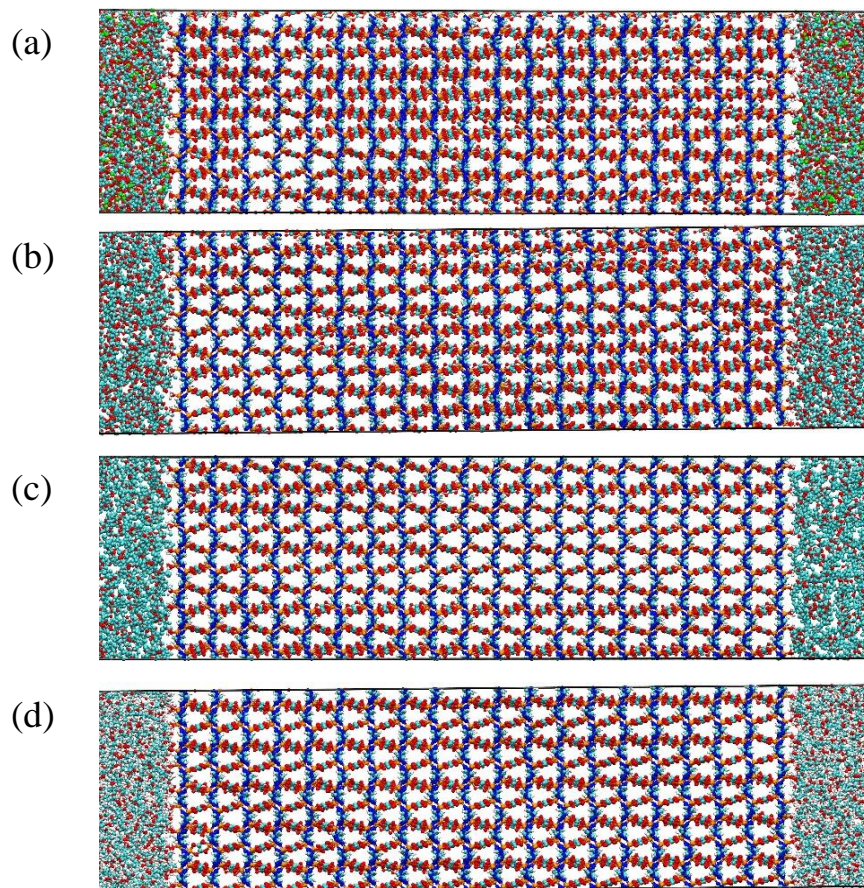


Figure S8 | Illustration of the atomistic models for (a) CMC/CALF-20, (b) PVA/CALF-20, (c) PVB/CALF-20, and (d) PVOH/CALF-20. Color scheme: Zn, Orange; O, red; N, blue; C, cyan; H, white. For the MD calculations, the MOF/polymer was unwrapped along the z-direction and the polymer slab was duplicated on each side of the MOF in such a way that the MOF was located between two polymer slabs 30 Å vacuum was further introduced in the z-direction to prevent mutual interactions between the polymers.

Table S14 | Length of the overlap regions of the composite, the error bar was calculated from the ensemble average.

System	Overlap Region (Å)
CMC/CALF-20	4.33 ± 0.47
PVA/CALF-20	3.83 ± 0.37
PVB/CALF-20	3.00 ± 0.00
PVOH/CALF-20	4.00 ± 0.58

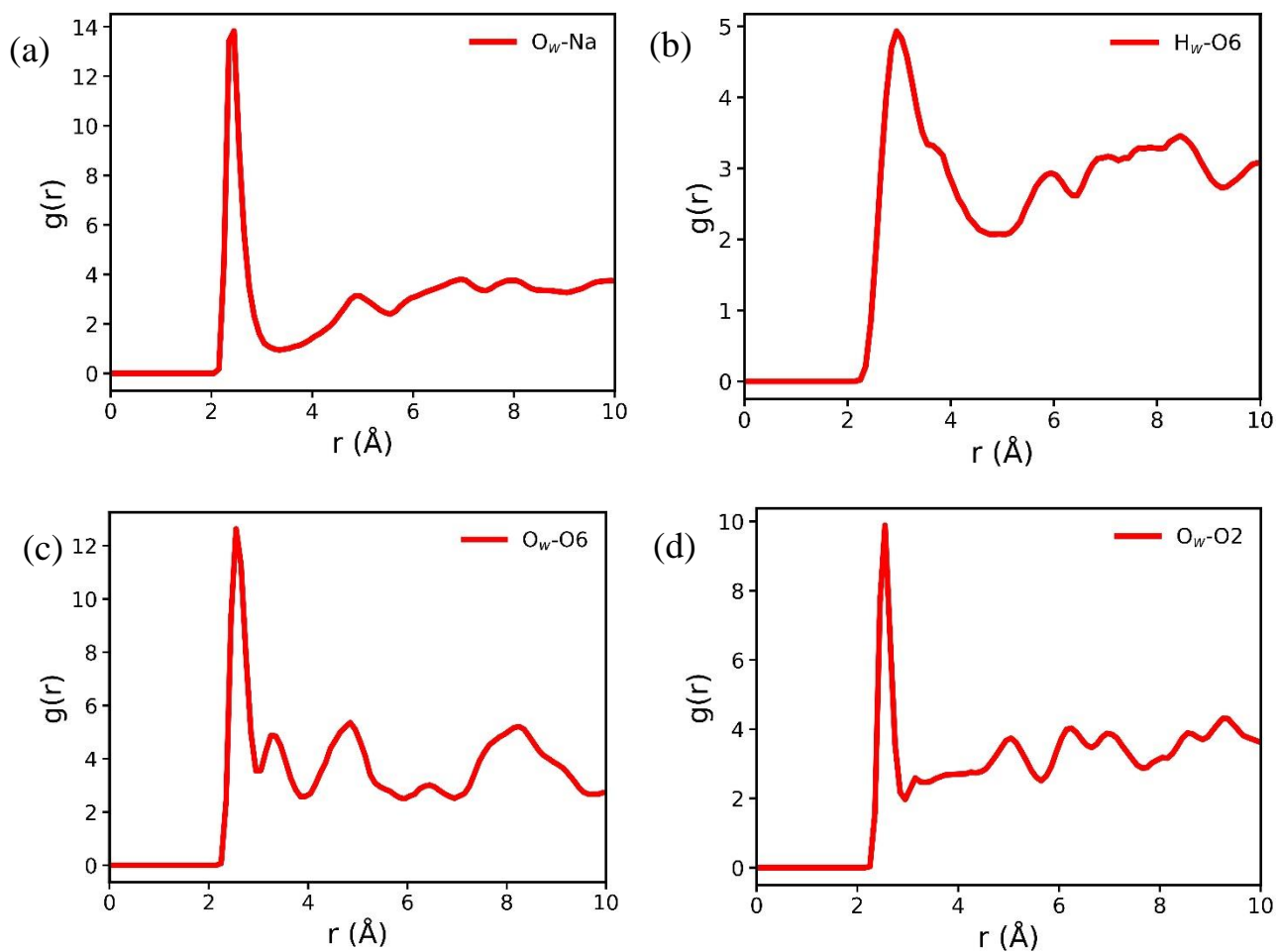


Figure S9 | Radial distribution functions calculated between the CMC binder and the CALF-20 in the composites. The oxygen and hydrogen atoms of the Zn-coordinated water are denoted by O_w and H_w respectively. The atom type of the CMC binder can be found in the Figure S1.

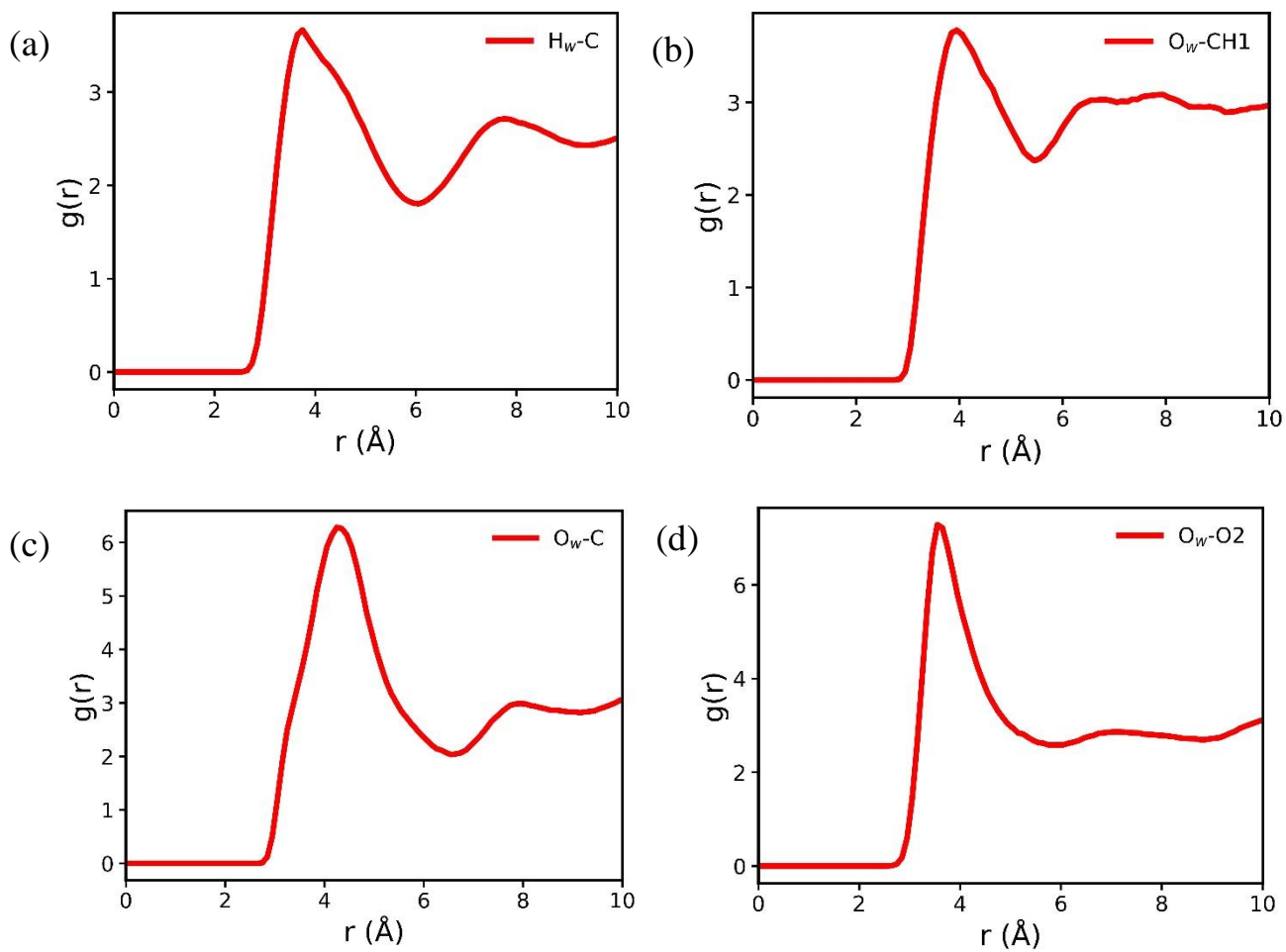


Figure S10 | Radial distribution function between the PVA binder and the CALF-20 in the composites. The oxygen and hydrogen atoms of the Zn-coordinated water are denoted by O_w and H_w respectively. The atom type of the PVA binder can be found in the figure S2.

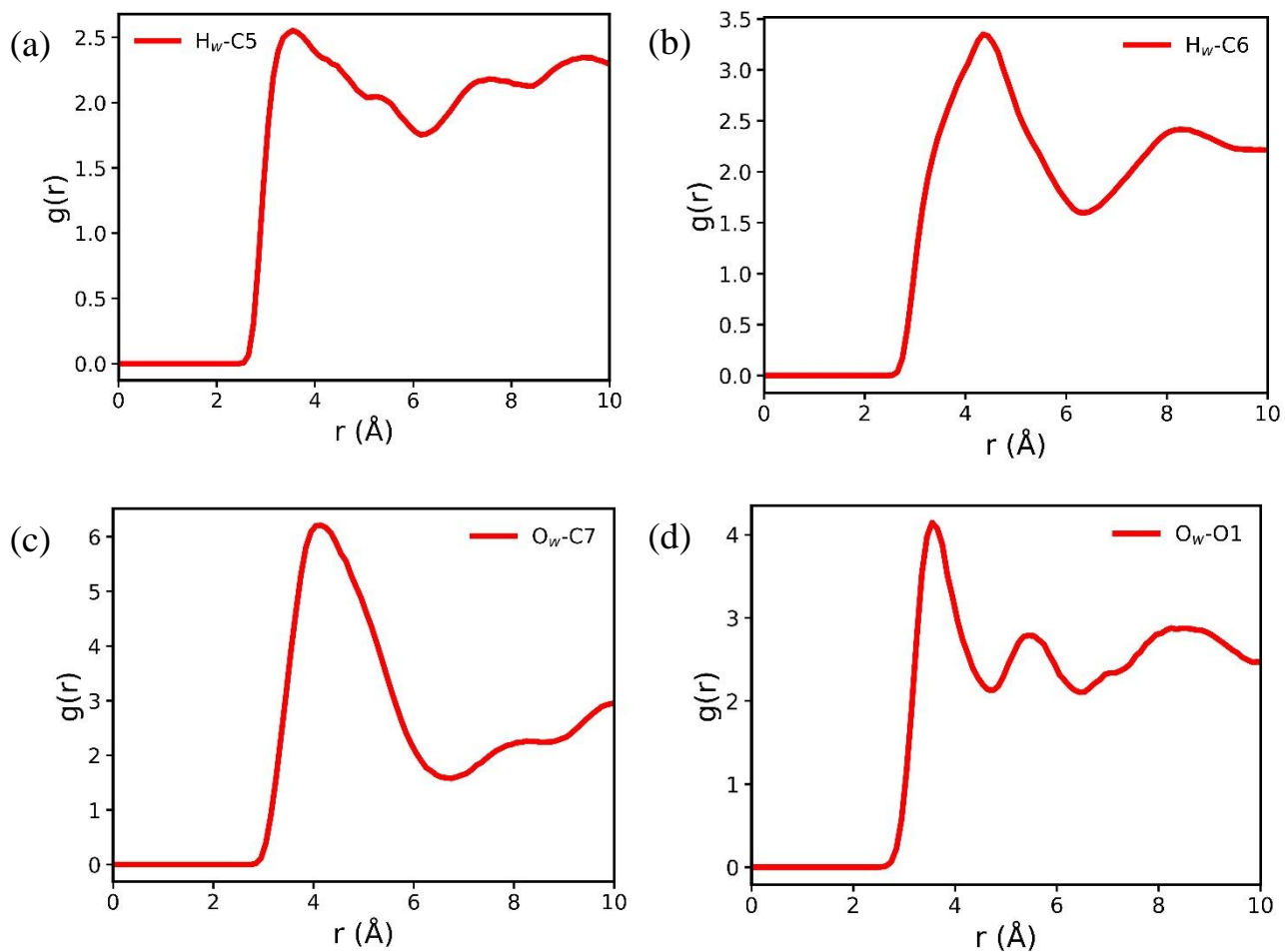


Figure S11 | Radial distribution function between the PVB binder and the CALF-20 in the composites. The oxygen and hydrogen atoms of the Zn-coordinated water is denoted by O_w and H_w respectively. The atom type of the PVB binder can be found in the Figure S3.

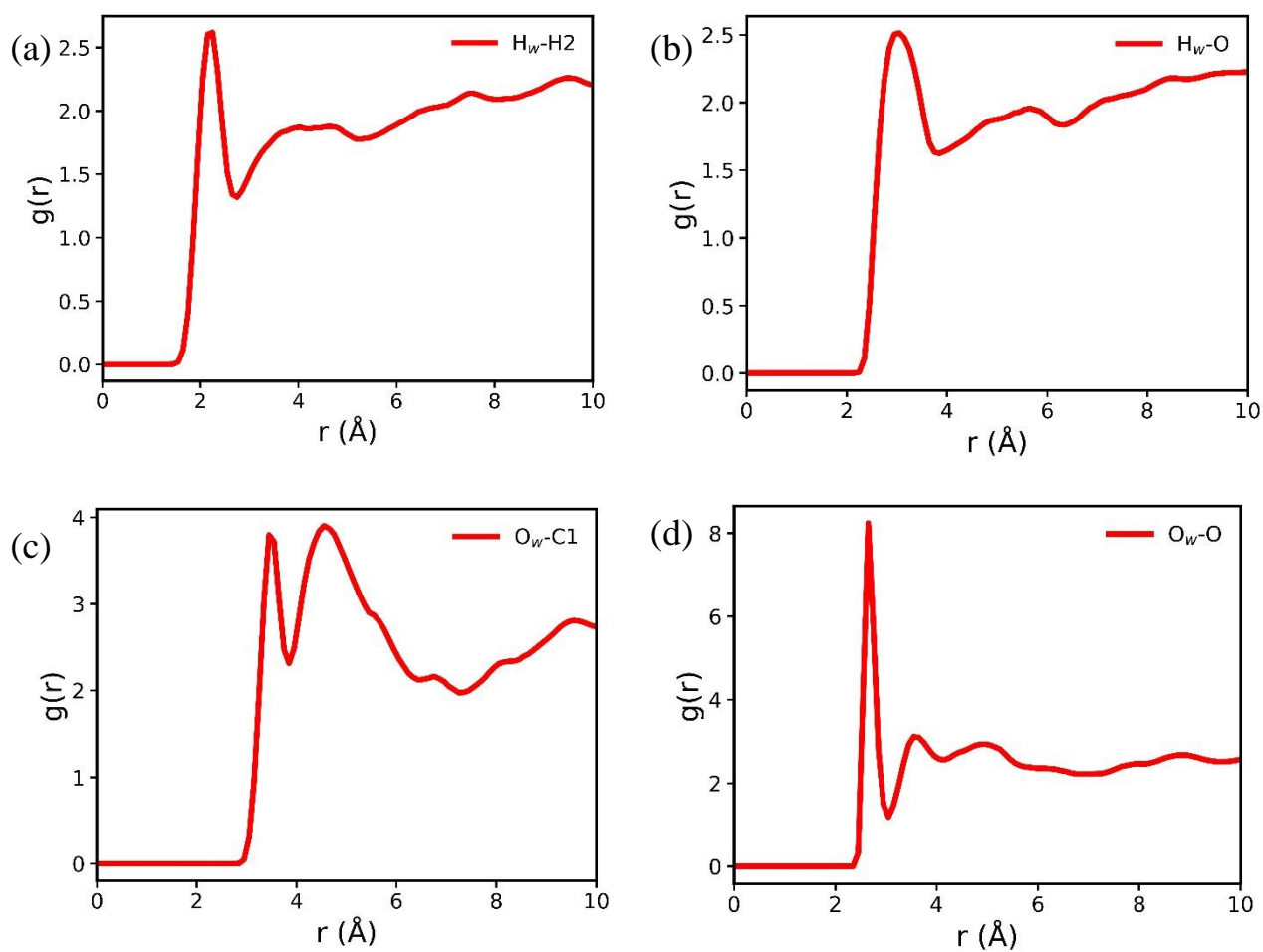


Figure S12 | Radial distribution function between the PVOH binder and the CALF-20 in the composites. The oxygen and hydrogen atoms of the Zn-coordinated water is denoted by O_w and H_w respectively. The atom type of the PVOH binder can be found in the Figure S4.

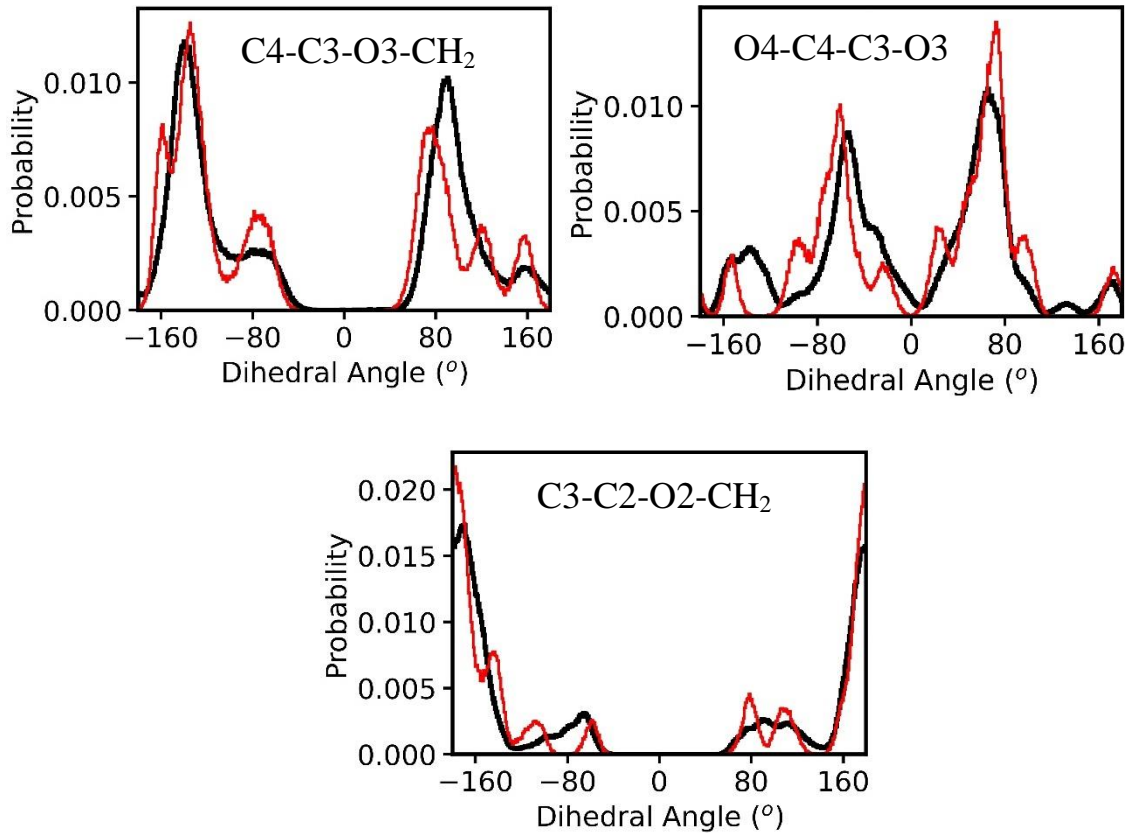


Figure S13 | Dihedral angle distribution for the CMC binder at the interface of CMC/CALF-20 composite and in the bulk region. Atom type can be found in the Figure S1. Black curve represents the dihedral angle distribution of the CMC binder in the bulk region whereas red curve represents the dihedral angle distribution of the CMC binder at the interface of the CMC/CALF-20 composite.

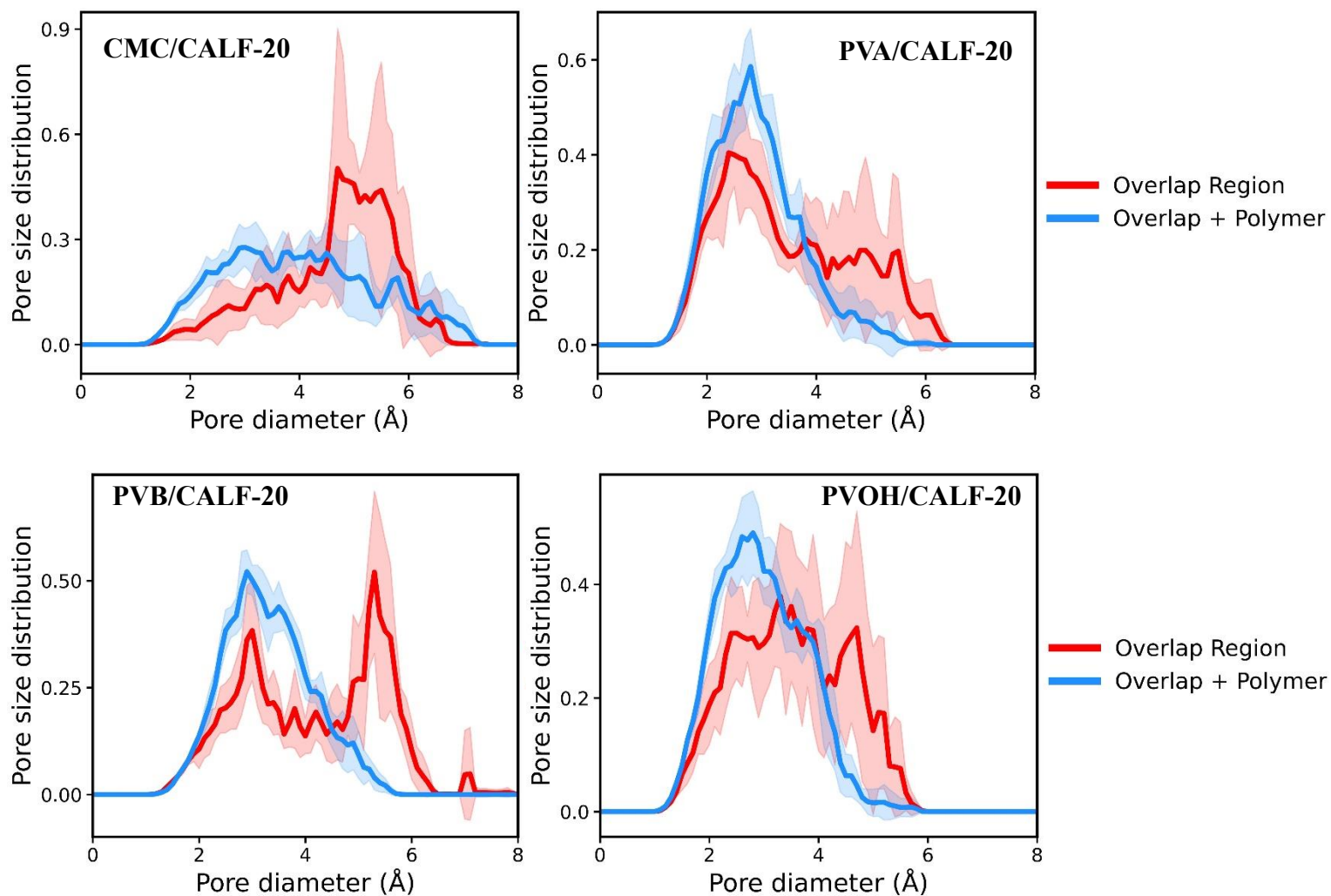


Figure S14 | Pore size distribution (PSD) of the binder in the overlap region of the interface of CALF-20/ binder composite and in the bulk binder region.

Table S15 | Force-field parameters for CO₂²⁴, N₂²⁵, CH₄²⁶

CO₂			
Atom	ϵ (kcal/mol)	σ (Å)	charge
C	0.05590	2.757	0.6512
O	0.15998	3.033	-0.3256

N₂			
Atom	ϵ (kcal/mol)	σ (Å)	charge
N	0.71539	3.31	-0.4820
Pseudo Atom	0.00000	0.00	0.9640

CH₄			
Atom	ϵ (kcal/mol)	σ (Å)	charge
CH ₄ (united atom)	0.29410	3.73	0.0

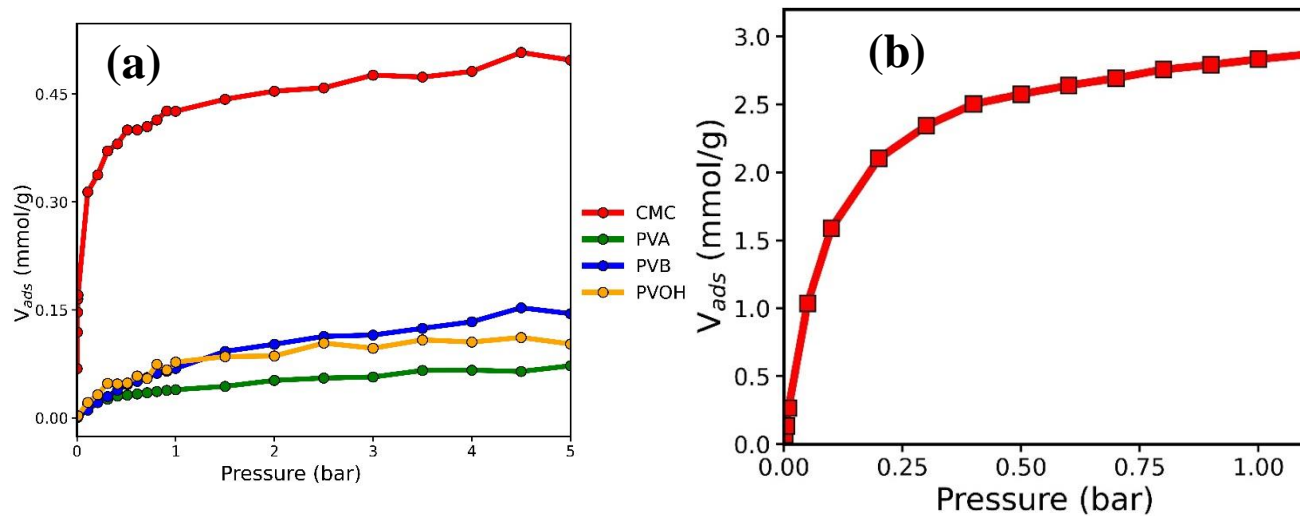


Figure S15 | GCMC simulated adsorption isotherms of CO₂ in (a) CMC, PVA, PVB, PVOH binders and (b) CALF-20 bulk structure at 300 K.

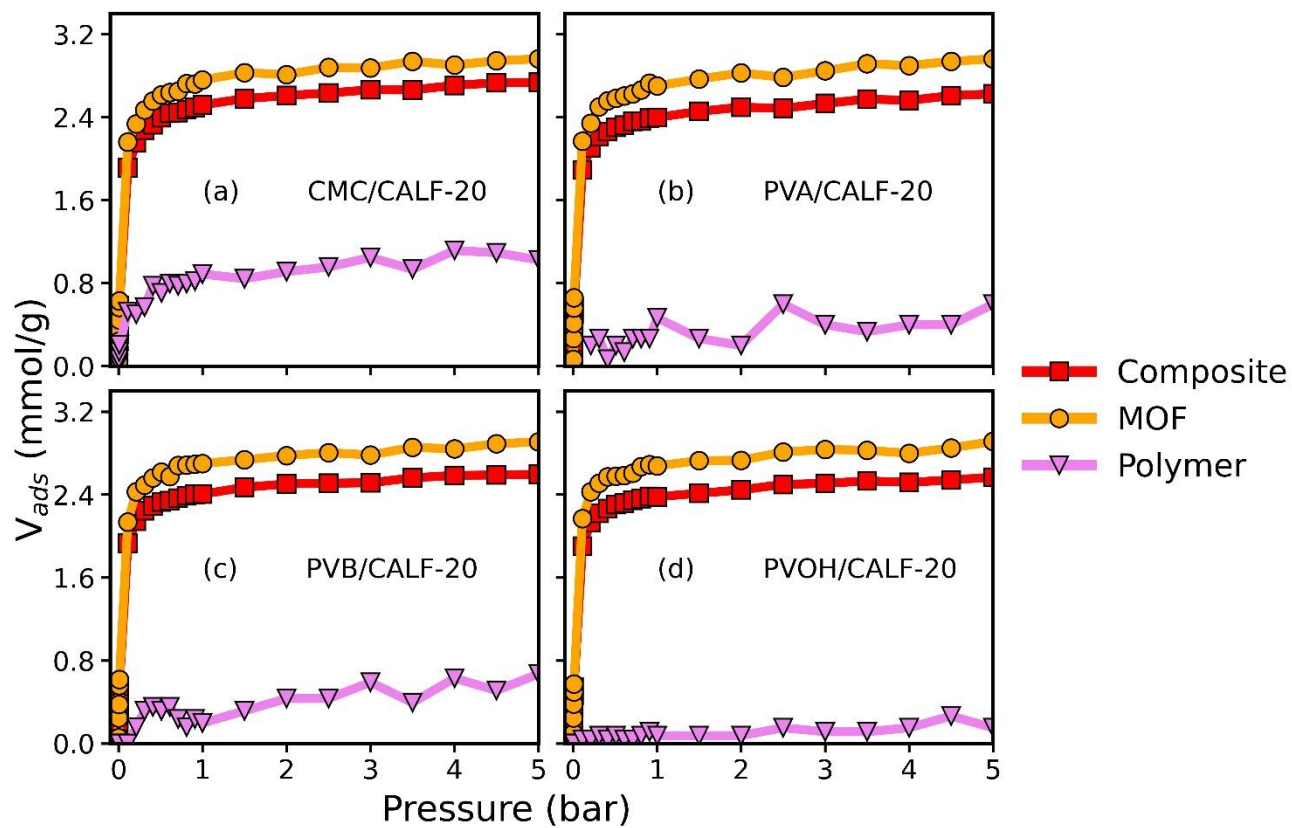


Figure S16 | GCMC simulated adsorption isotherms of CO₂ in CALF-20/binder composites. The amount of CO₂ adsorbed separately by the MOF and binder is also illustrated in the results.

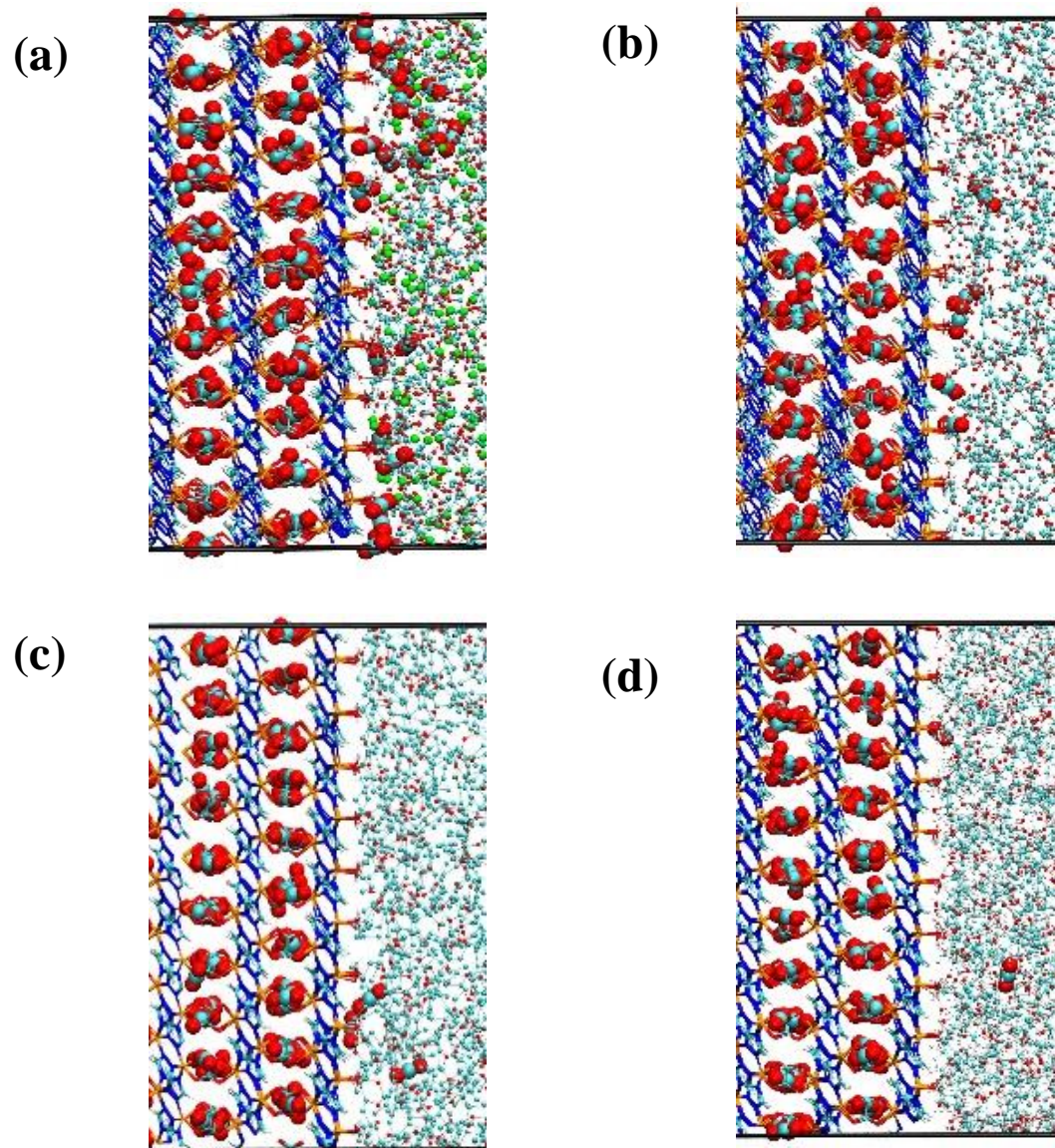


Figure S17 | Snapshots of the GCMC loaded CO₂ composites at 300 K and 1 bar (a) CMC/CALF-20, (b) PVA/CALF-20, (c) PVB/CALF-20, and (d) PVOH/CALF-20 composites.

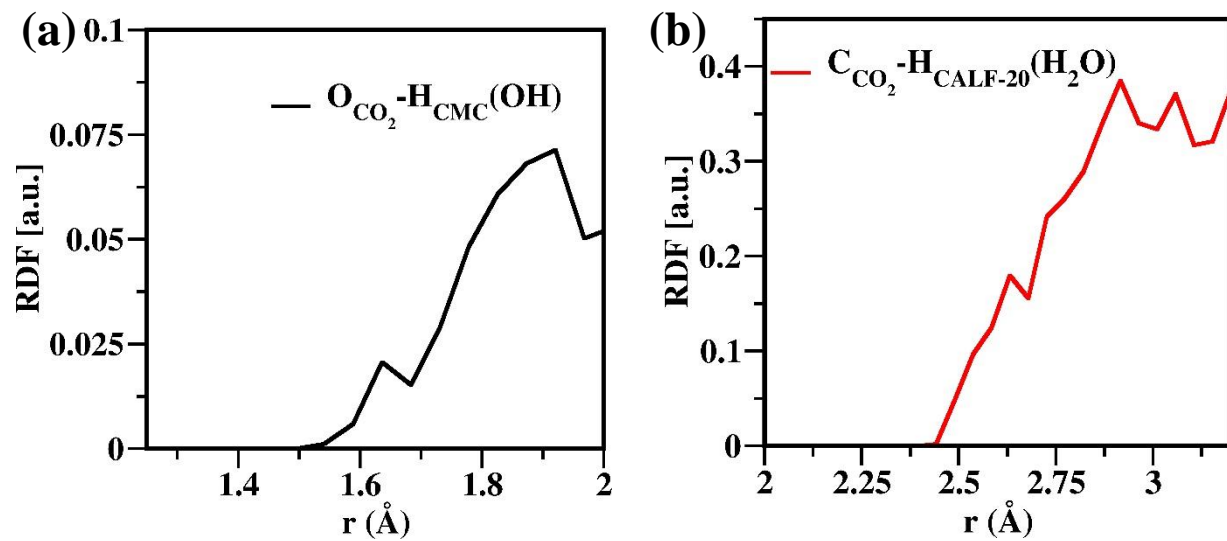


Figure S18 | RDFs corresponding to the most prominent interactions between CO₂ and the CALF-20/CMC composite from GCMC simulation at 1 bar and 300 K.

Diffusion of CO₂ inside CALF-20

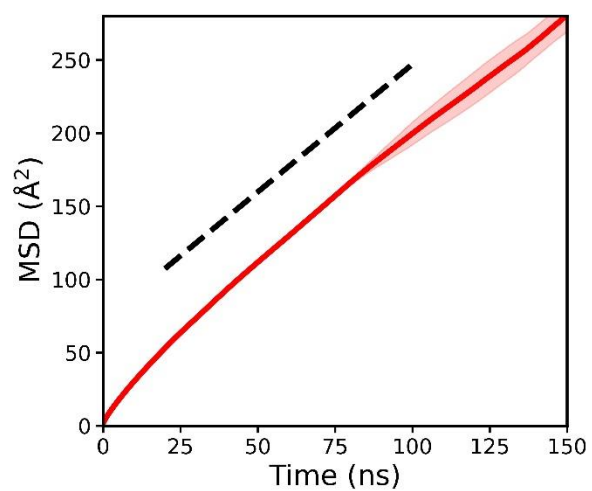


Figure S19 | Mean-squared displacement of the CO₂ molecule in CALF-20 region from the composite at 300 K and 1 bar. Only those CO₂ molecules that are residing inside the CALF-20 region during the simulation timescale are considered for MSD calculation.

References

1. Biermann, O., Hädicke, E., Koltzenburg, S. & Müller-Plathe, F. Hydrophilicity and Lipophilicity of Cellulose Crystal Surfaces. *Angewandte Chemie International Edition* **40**, 3822–3825 (2001).
2. Dong, X., Guan, X., Jiang, Y., Ma, J. & Zhang, M. Extension of the TraPPE-UA force field to the simulation of vapor–liquid phase equilibria of vinyl acetate system. *J Mol Liq* **209**, 520–525 (2015).
3. Semino, R., Dürholt, J. P., Schmid, R. & Maurin, G. Multiscale Modeling of the HKUST-1/Poly(vinyl alcohol) Interface: From an Atomistic to a Coarse Graining Approach. *J Phys Chem C* **121**, 21491–21496 (2017).
4. Wang, J., Wolf, R. M., Caldwell, J. W., Kollman, P. A. & Case, D. A. Development and testing of a general Amber force field. *J Comput Chem* **25**, 1157–1174 (2004).
5. Hofmann, D. L. F. J. U. C. S. and M. B. Detailed-atomistic molecular modeling of small molecule diffusion and solution processes in polymeric membrane materials Online Library. *Macromolecular theory and simulations* 293–327 [https://onlinelibrary.wiley.com/doi/10.1002/1521-3919\(20000701\)9:6%3C293::AID-MATS293%3E3.0.CO;2-1](https://onlinelibrary.wiley.com/doi/10.1002/1521-3919(20000701)9:6%3C293::AID-MATS293%3E3.0.CO;2-1) (2000).
6. Karayiannis, N. C., Mavrantzas, V. G. & Theodorou, D. N. Detailed Atomistic Simulation of the Segmental Dynamics and Barrier Properties of Amorphous Poly(ethylene terephthalate) and Poly(ethylene isophthalate). *Macromolecules* **37**, 2978–2995 (2004).
7. Larsen, G. S., Lin, P., Hart, K. E. & Colina, C. M. Molecular simulations of pim-1-like polymers of intrinsic microporosity. *Macromolecules* **44**, 6944–6951 (2011).
8. Ruchhoft, C. C. & Meckler, C. Carboxymethylcellulose. Uses and Applications. *Ind Eng Chem* **37**, 943–947 (1945).
9. Ma, H. & Ma, Q. Experimental Studies on the Mechanical Properties of Loess Stabilized with Sodium Carboxymethyl Cellulose. *Advances in Materials Science and Engineering* **2019**, 1–8 (2019).
10. Composition of POLYVINYL ACETATE. <https://pml.nist.gov/cgi-bin/Star/compos.pl?matno=229>.
11. Bicerano, J. Prediction of Polymer Properties. *Prediction of Polymer Properties* (2002) doi:10.1201/9780203910115.

12. Composition of POLYVINYL BUTYRAL. <https://physics.nist.gov/cgi-bin/Star/compos.pl?matno=231>.
13. Composition of POLYVINYL ALCOHOL. <https://pml.nist.gov/cgi-bin/Star/compos.pl?matno=230>.
14. Guo, T. *et al.* Bioinspired self-assembled films of carboxymethyl cellulose–dopamine/montmorillonite. *J Mater Chem A Mater* **7**, 14033–14041 (2019).
15. Eivazzadeh-Keihan, R. *et al.* Hybrid Bionanocomposite Containing Magnesium Hydroxide Nanoparticles Embedded in a Carboxymethyl Cellulose Hydrogel plus Silk Fibroin as a Scaffold for Wound Dressing Applications. *ACS Appl Mater Interfaces* **13**, 33840–33849 (2021).
16. Layek, R. K., Kuila, A., Chatterjee, D. P. & Nandi, A. K. Amphiphilic poly(N-vinyl pyrrolidone) grafted graphene by reversible addition and fragmentation polymerization and the reinforcement of poly(vinyl acetate) films. *J Mater Chem A Mater* **1**, 10863 (2013).
17. Khan, U., May, P., Porwal, H., Nawaz, K. & Coleman, J. N. Improved adhesive strength and toughness of polyvinyl acetate glue on addition of small quantities of graphene. *ACS Appl Mater Interfaces* **5**, 1423–1428 (2013).
18. Nakane, K., Kurita, T., Ogihara, T. & Ogata, N. Properties of poly(vinyl butyral)/TiO₂ nanocomposites formed by sol–gel process. *Compos B Eng* **35**, 219–222 (2004).
19. Bai, Y., Chen, Y., Wang, Q. & Wang, T. Poly(vinyl butyral) based polymer networks with dual-responsive shape memory and self-healing properties. *J Mater Chem A Mater* **2**, 9169 (2014).
20. Yamaura, K., Tada, M., Tanigami, T. & Matsuzawa, S. Mechanical properties of films of poly(vinyl alcohol) derived from vinyl trifluoroacetate. *J Appl Polym Sci* **31**, 493–500 (1986).
21. J. Brandrup, E. H. I. and E. A. G. Polymer Handbook 2 Volumes Set. 2366 (1999).
22. Lin, J. bin *et al.* A scalable metal-organic framework as a durable physisorbent for carbon dioxide capture. *Science (1979)* **374**, 1464–1469 (2021).
23. Rappé, A. K., Casewit, C. J., Colwell, K. S., Goddard, W. A. & Skiff, W. M. UFF, a Full Periodic Table Force Field for Molecular Mechanics and Molecular Dynamics Simulations. *J Am Chem Soc* **114**, 10024–10035 (1992).
24. Harris, J. G. & Yung, K. H. Carbon Dioxide’s Liquid-Vapor Coexistence Curve And Critical Properties as Predicted by a Simple Molecular Model. *J Phys Chem* **99**, 12021–12024 (1995).

25. Potoff, J. J. & Siepmann, J. I. Vapor-liquid equilibria of mixtures containing alkanes, carbon dioxide, and nitrogen. *AIChE Journal* **47**, 1676–1682 (2001).
26. Martin, M. G. & Siepmann, J. I. Transferable Potentials for Phase Equilibria. 1. United-Atom Description of n-Alkanes. *J. Phys. Chem. B* **102**, 2569–2577 (1998).